High-Temperature Thermal Decomposition of Isobutane and *n*-Butane Behind Shock Waves

Matthew A. Oehlschlaeger,* David F. Davidson, and Ronald K. Hanson

High-Temperature Gasdynamics Laboratory, Department of Mechanical Engineering, Stanford University, Stanford, California, 94305-3032

Received: December 31, 2003; In Final Form: February 27, 2004

The decomposition rates of isobutane and *n*-butane in the falloff regime at high temperatures were studied in a shock tube using UV narrow-line laser absorption of CH_3 at 216.6 nm. Experimental conditions ranged from 1297 to 1601 K and 0.20 to 8.8 atm with mixtures varying in concentration from 198 to 400 ppm of isobutane or *n*-butane diluted in argon. Decomposition rate coefficients were determined by monitoring the formation rate of CH_3 immediately behind shock waves and modeling the CH_3 formation with detailed kinetic mechanisms. Calculations were performed using RRKM/master equation analysis with a restricted (hindered) Gorin model for the transition state and fit to the experimental data. The rate coefficient for isobutane decomposition, $i\text{-}C_4H_{10} \rightarrow CH_3 + i\text{-}C_3H_7$, from 1320 to 1560 K can be described, using the Troe pressure-broadening formulation, by $k_{\infty,1}(T) = 4.83 \times 10^{16} \exp(-402\ 10\ \text{K}/T)\ \text{s}^{-1}$, $k_{0,1}(T) = 2.41 \times 10^{19} \exp(-264\ 60\ \text{K}/T)\ \text{cm}^3\ \text{mol}^{-1}\ \text{s}^{-1}$, and $F_{\text{cent},1}(T) = 0.75 \exp(-T/750\ \text{K})$. *n*-Butane decomposes via two reaction routes. The rate coefficient for $n\text{-}C_4H_{10} \rightarrow CH_3 + n\text{-}C_3H_7$ from 1320 to 1600 K can be described by $k_{\infty,2}(T) = 4.28 \times 10^{14} \exp(-351\ 80\ \text{K}/T)\ \text{s}^{-1}$, $k_{0,2}(T) = 5.34 \times 10^{17} \exp(-216\ 20\ \text{K}/T)\ \text{cm}^3\ \text{mol}^{-1}\ \text{s}^{-1}$, and $F_{\text{cent},2}(T) = 0.28 \exp(-T/1500\ \text{K})$. And the rate coefficient for $n\text{-}C_4H_{10} \rightarrow C_2H_5 + C_2H_5$ from 1320 to 1600 K can be described by $k_{\infty,3}(T) = 2.72 \times 10^{15} \exp(-380\ 50\ \text{K}/T)\ \text{s}^{-1}$, $k_{0,3}(T) = 4.72 \times 10^{18} \exp(-249\ 50\ \text{K}/T)\ \text{cm}^3\ \text{mol}^{-1}\ \text{s}^{-1}$, and $F_{\text{cent},3}(T) = 0.28 \exp(-T/1500\ \text{K})$.

Introduction

The decomposition reactions for isobutane and *n*-butane are important initiation steps in the detailed reaction mechanisms describing the high-temperature oxidation of these two fuels. Furthermore, global combustion parameters, such as ignition times, show strong sensitivity to these reactions.[1,2] With the development of a CH_3 laser absorption diagnostic at 216.6 nm, detailed measurements of the following reactions are possible at high temperatures:

$$i\text{-}C_4H_{10} \rightarrow CH_3 + i\text{-}C_3H_7 \quad (1)$$

$$n\text{-}C_4H_{10} \rightarrow CH_3 + n\text{-}C_3H_7 \quad (2)$$

$$n\text{-}C_4H_{10} \rightarrow C_2H_5 + C_2H_5 \quad (3)$$

Previous rate coefficient determinations for reactions 1−3 are scarce in comparison to the large body of work performed on ethane and propane decomposition.[3] Additionally, much of the previous data is of uncertain reliability due to the large initial concentrations of reactant used (1−2.8%) that can cause interfering reactions to complicate the determination of decomposition rate coefficients.

Reaction 1 has been studied previously using single-pulse shock tube techniques,[4] 3.39 μm laser absorption of isobutane,[5] and UV lamp absorption of CH_3.[6] There has been only one high-temperature study of reaction 2, and this employed UV lamp absorption of CH_3.[7] The reaction 3 rate coefficient has not been previously determined at high temperatures, to our knowledge, but there have been several low-temperature studies performed primarily in flow tubes.[8−10]

In this work we present measurements of k_1-k_3 using narrow-linewidth laser absorption for ppm-sensitive CH_3 detection. The experiments are dilute enough to maintain excellent sensitivity to the rate coefficients of interest and of sufficient concentration (198−400 ppm) to be insensitive to impurities. The analysis focuses only on the early-time behavior of the CH_3 profiles in order to maintain isolation of the decomposition reactions and to avoid interfering absorption from other product species that are formed at longer times.

In addition, the current experimental data has been fit using calculations based on an RRKM/1-D (internal energy) master equation approach using a restricted Gorin model for the transition states.[11,12] These experiments and fits provide determinations of the high-pressure limiting rate coefficients. The analysis reveals a strong positive temperature dependence of $<\Delta E>_{\text{down}}$ (collisional energy transfer parameter). Analytic expressions for k_∞, k_0, and F_{cent} were determined for reactions 1−3, using the Troe formulation for pressure broadening. Finally, the current determinations for k_3 along with previously determined rates for ethane and propane decomposition[3] allow for a test of the validity of the geometric mean rule.

Experimental Section

Apparatus. The experiments reported here were performed behind both incident and reflected shock waves in a pressure-driven stainless steel shock tube. The driven section is 8.54 m long, and the driver is 3.35 m long; both sections are 14.13 cm in inner diameter. The driven-section vacuum system consists of a zeolite-trapped mechanical pump and a Varian V-250 turbomolecular pump, providing ultimate pressures of 10^{-7} Torr

* Corresponding author. Address: Stanford University, Bldg 520, Room 520I, Stanford, CA 94305-3032. Phone: 650-725-6771. Fax: 650-723-1748. E-mail: moehlsch@stanford.edu.

10.1021/jp0313627 CCC: $27.50
Published on Web 04/20/2004

with a typical leak rate of 10^{-6} Torr per minute. Shock velocities were extrapolated to the endwall from four incident shock wave velocity measurements made with piezo pressure transducers over the last 1.5 m of the shock tube. The preshock initial mixture pressure was measured using a high-accuracy Baratron pressure transducer. The incident and reflected shock conditions were calculated using the normal shock equations; uncertainty in the experimental pressure and temperature are 1.1% and 0.6%, respectively, with the primary contribution being the uncertainty in the measured shock velocity. Mixtures were made in a turbo-pumped stainless steel mixing chamber with an internal stirring system. Research grade argon (99.999%) was used as the driven carrier gas and helium was used as the driver gas. Isobutane and *n*-butane were provided by Aldrich and Praxair respectively in purities of 99+%.

CH_3 Diagnostic. Methyl radicals (CH_3) were monitored during these experiments using laser absorption at 216.6 nm. Laser light at 433.2 nm was created by pumping a Coherent 699 ring dye laser, operating on stilbene 420 dye, with 7 W (all-lines UV) from a Coherent Innova 25/7 Ar^+ laser. The output of the dye laser was then frequency-doubled in a Spectra-Physics Wavetrain external doubling cavity using an angle-tuned BBO crystal. The wavelength was monitored by passing a portion of the dye laser output (undoubled) into a wavemeter; mode quality was monitored by passing a portion through a scanning interferometer.

The doubled UV beam (2−3 mW at 216.6 nm) was passed to the shock tube where it was split into two components: one was passed through the shock tube to be absorbed by CH_3 (I), the other was detected prior to absorption as a reference (I_0). These two beams were detected using amplified S1722-02 Hamamatsu silicon photodiodes (rise time <0.5 μs, 4.1 mm diameter) and recorded on a digital oscilloscope.

The CH_3 $B(^2A'_1) \leftarrow X(^2A''_2)$ transition has an absorption maximum at 216.6 nm.[13] The absorption coefficient at this wavelength has been previously measured by Davidson et al.[14] Prior to performing the current experiments the temperature dependence of the absorption coefficient was investigated once again. Dilute mixtures (200 ppm) of azomethane, methyl iodide, and ethane were shock heated to produce known, instantaneous postshock CH_3 yields. The absorption coefficient was determined by measuring the time-zero absorption of the immediate CH_3 yield. These most recent measurements differ by no more than 10% with those of Davidson et al.[14] and have about a factor of 2 less experimental scatter. A least-squares fit to our most recent absorption coefficient data over the range 1200−2500 K is given by

$$k_{\lambda,\mathrm{CH3}} = 1.475 \times 10^4\, T^{-1.004} \exp(2109\ \mathrm{K}/T)\ \mathrm{atm}^{-1}\ \mathrm{cm}^{-1}$$

with a 2σ least-squares deviation of ±5% in the data. The absorption coefficient shows no pressure dependence across the range of pressures employed in this study.

The CH_3 mole fraction in a given experiment can be determined using Beer's law: $I/I_0 = \exp(-k_\lambda P X_{\mathrm{CH3}} L)$, where I is the intensity of the absorbed UV beam and I_0 is the intensity of the reference beam, k_λ is the temperature-dependent absorption coefficient ($\mathrm{atm}^{-1}\ \mathrm{cm}^{-1}$) at the wavelength λ, P is the total pressure (atm), X_{CH3} is the mole fraction of the absorbing species, CH_3, and L is the shock tube diameter (14.13 cm). The CH_3 diagnostic provides a minimum detectivity of 0.1% absorbance ($\ln(I_0/I) = 0.001$) and thus is capable of ppm CH_3 detection.

Method for Determination of Rate Coefficients. In order to determine rate coefficients for reactions 1−3, the measured

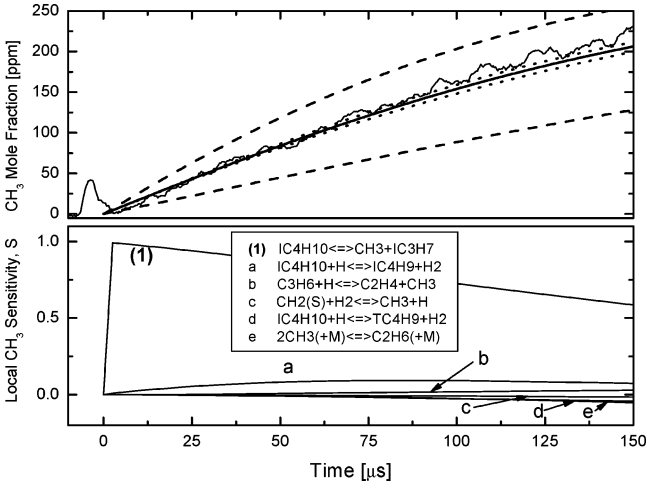

Figure 1. Example isobutane data, modeling (top), and sensitivity (bottom). Incident shock conditions: 1401 K, 0.238 atm, 400 ppm i-C_4H_{10}/Ar. Top graph: solid line, fit to data using the Wang et al.[15] mechanism and adjusting k_1; dashed lines, variation of k_1 ±50%; dotted lines, variation of rate coefficient for i-$C_4H_{10} + H \rightarrow i$-$C_4H_9 + H_2$ by ±50%. $S = (\mathrm{d}X_{\mathrm{CH3}}/\mathrm{d}k_i)\ (k_i/X_{\mathrm{CH3,local}})$, where k_i is the rate constant for reaction i and $X_{\mathrm{CH3,local}}$ is the local CH_3 mole fraction.

CH_3 mole fractions were fit using detailed kinetic mechanisms. The mechanism of Wang et al.[15] was used for isobutane decomposition; this mechanism although originally designed to model neopentane oxidation contains all of the necessary chemistry to model isobutane decomposition. The mechanism of Marinov et al.[16] was used for *n*-butane decomposition. Fortunately, the low initial fuel concentrations used in these experiments allowed fits that are quite insensitive to the choice of the other rate coefficients. The only rate coefficients changed in the mechanism, for the purpose of fitting these data, are those of reactions 1−3. Computations were done using CHEMKIN 2.0 and SENKIN.[17,18]

In the case of isobutane the kinetic modeling is quite simple, the initial rise of CH_3 provides a direct fit to reaction 1, as there is only one decomposition route for the conditions of these experiments. The rate coefficient was fit only to the early-time behavior of the CH_3 traces; at longer times, a complication arises from interfering absorption. Example data and sensitivity are given in Figure 1; notice that the model fits the first 75 μs of the trace well but then diverges slightly from the experiment at longer times due to interfering absorption.

Experiments were performed to identify possible interfering absorbing species (C_3H_6, C_2H_4, and C_2H_2). The absorption coefficients of these species at 216.6 nm were measured by monitoring 216.6 nm laser absorption during shock heating. It was found that although none of these species had absorption coefficients large enough to be of concern, the decomposition products of C_3H_6 showed moderately strong absorption. These C_3 decomposition products are likely responsible for the interference in the isobutane decomposition experiments; similar interference was reported by Koike and Morinaga.[6]

Analysis of the CH_3 profiles obtained from the *n*-butane experiments is complicated by the fact that there are two parallel channels for *n*-butane decomposition, reactions 2 and 3, and thus the CH_3 profiles must be fit in terms of the overall decomposition rate coefficient, $k_2 + k_3$, and the branching ratio, $k_2/(k_2 + k_3)$. The overall rate of decomposition, $k_2 + k_3$, is determined by fitting to the initial slope of the CH_3 concentration profile. At longer times the CH_3 concentration rolls off to a peak before methyl−methyl recombination brings about a decrease in the CH_3 concentration. The peak in the methyl

TABLE 1: Summary of Experimental Results

T [K]	P [atm]	k_1 [1/s]	T [K]	P [atm]	k_2 [1/s]	k_3 [1/s]
initial $X_{i-C4H10}$: 400 ppm[a]			initial $X_{n-C4H10}$: 399 ppm[a]			
1352	0.251	1.8×10^3	1337	0.250	7.0×10^2	6.0×10^2
1401	0.238	4.4×10^3	1432	0.226	3.5×10^3	2.0×10^3
1458	0.224	9.5×10^3	1500	0.213	8.5×10^3	6.8×10^3
1539	0.212	2.8×10^4	1560	0.203	1.5×10^4	1.2×10^4
initial $X_{i-C4H10}$: 201 ppm			1381	0.235	1.5×10^3	1.2×10^3
1417	1.731	1.1×10^4	initial $X_{n-C4H10}$: 200 ppm			
1365	1.785	4.5×10^3	1479	1.673	1.3×10^4	1.3×10^4
1310	1.815	1.3×10^3	1601	1.677	4.5×10^4	4.5×10^4
1468	1.623	2.8×10^4	1436	1.752	5.5×10^3	4.8×10^3
1483	1.660	3.2×10^4	1344	1.869	9.0×10^2	6.0×10^2
1551	1.607	8.0×10^4	1541	1.659	2.3×10^4	2.2×10^4
initial $X_{i-C4H10}$: 200 ppm			1360	1.786	1.4×10^3	1.0×10^3
1395	4.318	9.0×10^3	initial $X_{n-C4H10}$: 198 ppm			
1392	4.510	9.0×10^3	1376	4.282	2.5×10^3	2.0×10^3
1344	4.480	3.0×10^3	1447	4.303	8.0×10^3	8.0×10^3
1469	4.432	3.4×10^4	1404	3.778	4.3×10^3	3.0×10^3
1522	4.244	7.2×10^4	1520	4.208	3.0×10^4	3.0×10^4
initial $X_{i-C4H10}$: 200 ppm			initial $X_{n-C4H10}$: 200 ppm			
1414	8.218	1.5×10^4	1414	8.183	5.0×10^3	5.0×10^3
1368	8.420	6.3×10^3	1344	8.340	1.3×10^3	1.0×10^3
1333	8.843	3.1×10^3	1297	8.411	5.0×10^2	3.0×10^2
1535	7.934	1.2×10^5	1479	8.064	1.4×10^4	1.2×10^4

[a] Indicates incident shock experiments.

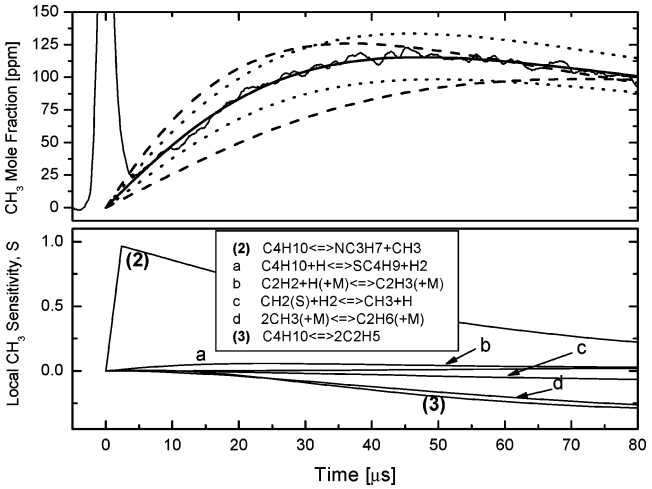

Figure 2. Example *n*-butane data, modeling (top), and sensitivity (bottom). Reflected shock conditions: 1479 K, 1.673 atm, 200 ppm *n*-C_4H_{10}/Ar. Top graph: solid line, fit to data using the Marinov et al.[16] mechanism and adjusting the overall decomposition rate, $k_2 + k_3$, and branching ratio, $k_2/(k_2 + k_3)$; dashed lines, variation of $k_2 + k_3$ ±50%; dotted lines, variation of $k_2/(k_2 + k_3)$ ±25%. $S = (dX_{CH3}/dk_i)(k_i/X_{CH3,local})$, where k_i is the rate constant for reaction i and $X_{CH3,local}$ is the local CH_3 mole fraction. The spike at 0 μs is caused by deflection of the diagnostic beam by the reflected shock wave.

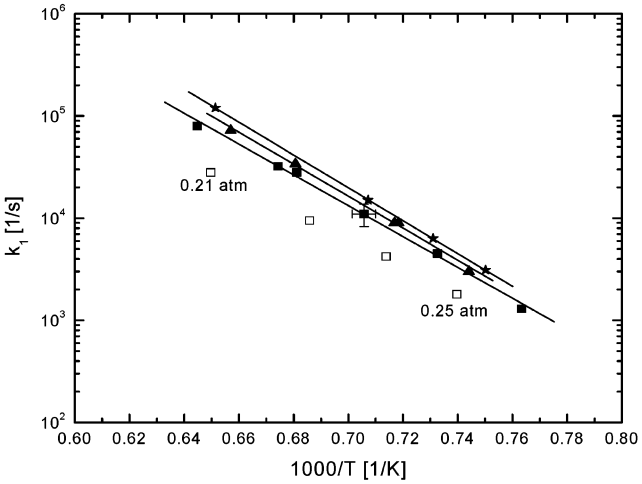

Figure 3. Experimental data and least-squares fits for *i*-$C_4H_{10} \rightarrow CH_3 + i$-$C_3H_7$. Filled squares, 1.7 atm data, $k_1 = 4.98 \times 10^{14} \exp(-348\ 00K/T)\ s^{-1}$; filled triangles, 4.4 atm data, $k_1 = 1.71 \times 10^{15} \exp(-363\ 00K/T)\ s^{-1}$; filled stars, 8.4 atm data, $k_1 = 3.59 \times 10^{15} \exp(-370\ 00K/T)\ s^{-1}$; open squares, 0.21−0.25 atm data.

concentration is controlled by the branching ratio, $k_2/(k_2 + k_3)$, and thus the branching ratio can be inferred by fitting to the peak in CH_3 concentration. See Figure 2 for an example data trace and sensitivity plot. Interfering chemistry at longer times provides a bit more uncertainty in the fits (sensitivity in Figure 2), but fortunately the primary interfering reaction is methyl recombination which is rather well-known (±20%). Interfering absorption is negligible in the *n*-butane decomposition case because the subsequent C_3 product fragments are in lower concentration than in the isobutane case.

The present rate coefficient determinations are tabulated in Table 1 and shown in Figures 3−5 on Arrhenius plots along with least-squares fits; the experimental scatter is small (±10% in k_1, ±20% in k_2, and ±30% in k_3). The primary contributions to uncertainties in the rate coefficients are: temperature (±10%), CH_3 absorption coefficient (±5%), fitting the data to computed profiles (±5−10%), and uncertainties resulting from interfering chemistry (±5% in k_1, ±15% in k_2, and ±15% in k_3). These uncertainties give overall uncertainties in k_1, k_2, and k_3 of ±25%, ±35%, and ±35% respectively.

RRKM Calculations

Single-channel (isobutane) and multichannel (*n*-butane) RRKM calculations with numerical solution to the 1-D (internal energy) master equation, to account for weak collision effects, were carried out using a restricted (hindered) Gorin model for the transition states of reactions 1−3 and fit to the current data set. The model locates the transition state at the maximum of an effective potential, using the Lennard-Jones form of the potential: $r^{\ddagger}/r = (6D_0/RT)^{1/6}$. The restricted Gorin transition state is similar to its product fragments. The transition state frequencies of vibration are assumed to be those of the product fragments, and internal rotations are represented by the moments

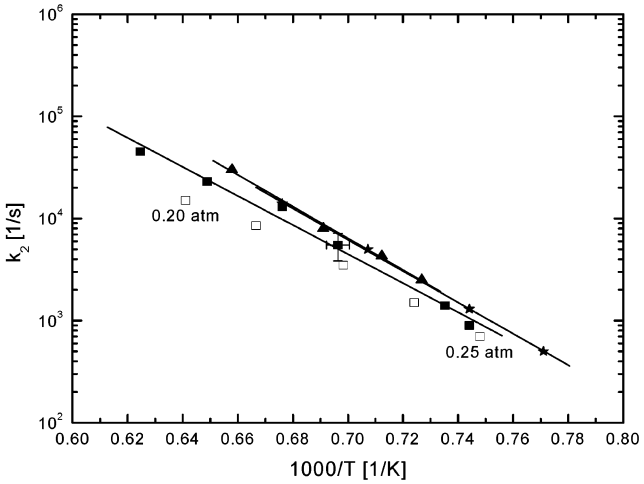

Figure 4. Experimental data and least-squares fits for n-$C_4H_{10} \rightarrow CH_3 + C_3H_7$. Filled squares, 1.7 atm data, $k_2 = 4.15 \times 10^{13}$ exp(−328 00K/T) s^{-1}; filled triangles, 4.2 atm data, $k_2 = 4.59 \times 10^{14}$ exp(−357 00K/T) s^{-1}; filled stars, 8.3 atm data, $k_2 = 3.33 \times 10^{14}$ exp(−353 00K/T) s^{-1}; open squares, 0.20−0.25 atm data.

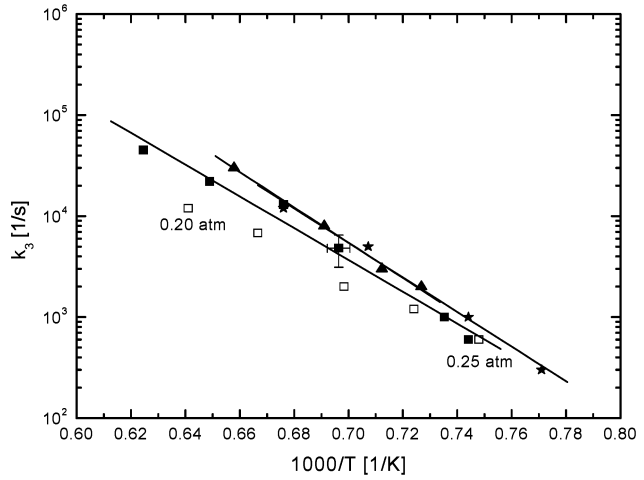

Figure 5. Experimental data and least-squares fits for n-$C_4H_{10} \rightarrow C_2H_5 + C_2H_5$. Filled squares, 1.7 atm data, $k_3 = 3.82 \times 10^{14}$ exp(−362 00K/T) s^{-1}; filled triangles, 4.2 atm data, $k_3 = 9.30 \times 10^{15}$ exp(−402 00K/T) s^{-1}; filled stars, 8.3 atm data, $k_3 = 5.21 \times 10^{15}$ exp(−394 00K/T) s^{-1}; open squares, 0.20−0.25 atm data.

of inertia of the product fragments with hindrance, η. The hindrance parameters, η, were chosen to reproduce the current data and are written in the functional form, $\eta = a + bT^{-1/6}$, suggested by previous workers;[11,12] expressions for the hindrance parameters are given in Table 2. Lennard-Jones parameters for isobutane, *n*-butane, and argon were taken from Hippler et al.;[19] the molecular frequencies, moments of inertia, heats of formation, and barrier heights were taken from various references[20−28] and are listed in Table 2.

The exponential-down collision energy transfer model was used with a temperature-dependent collisional energy transfer parameter which was fit to the current experiments. The resulting expressions for the energy collisional transfer parameter for argon collisions with isobutane and *n*-butane respectively are: $\langle\Delta E\rangle_{down} = 0.8 \times (T\ [K])\ cm^{-1}$ (isobutane) and $\langle\Delta E\rangle_{down} = 1.2 \times (T\ [K])\ cm^{-1}$ (*n*-butane). The falloff behavior of the current experiments could not be accurately fit without a temperature-dependent $\langle\Delta E\rangle_{down}$; similar results have been found by Klippenstein and Harding,[29] Knyazev and Slagle,[30,31] and Knyazev and Tsang.[32] The RRKM/1-D master equation

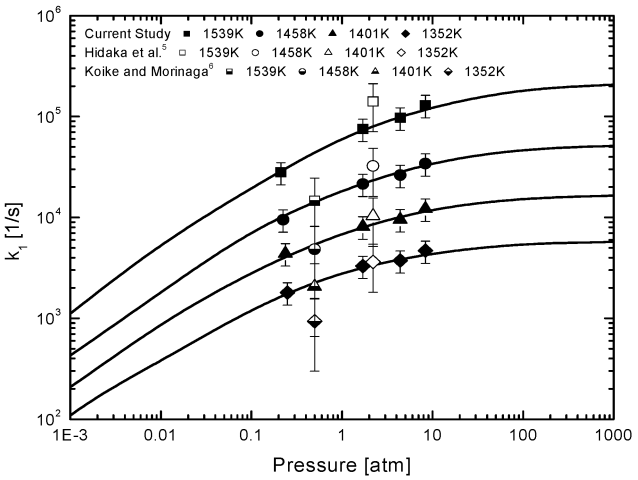

Figure 6. Falloff plot for i-$C_4H_{10} \rightarrow CH_3 + i$-$C_3H_7$. Solid symbols, current study; open symbols, Hidaka et al.;[5] half-filled symbols, Koike and Morinaga;[6] solid lines, RRKM/master equation results with $\langle\Delta E\rangle_{down} = 0.8 \times (T\ [K])\ cm^{-1}$.

calculations were performed with the Multiwell code of Barker.[33]

The RRKM/master equation calculations provided falloff curves for the rate coefficients for reactions 1−3. Analytic expressions for k_1−k_3, in the Troe formulation, were fit to the RRKM results; these expressions differ from the RRKM results by no more than ±10%. The reaction 1 rate expressions for 1320−1560 K are

$$k_{\infty,1}(T) = 4.83 \times 10^{16} \exp(-40210\ K/T)\ [s^{-1}]$$

$$k_{0,1}(T) = 2.41 \times 10^{19} \exp(-26460\ K/T)\ [cm^3 mol^{-1} s^{-1}]$$

$$F_{cent,1}(T) = 0.75 \exp(-T/750\ K)$$

The reaction 2 rate expressions for 1320−1600 K are

$$k_{\infty,2}(T) = 4.28 \times 10^{14} \exp(-35180\ K/T)\ [s^{-1}]$$

$$k_{0,2}(T) = 5.34 \times 10^{17} \exp(-21620\ K/T)\ [cm^3 mol^{-1} s^{-1}]$$

$$F_{cent,2}(T) = 0.28 \exp(-T/1500\ K)$$

And the reaction 3 rate expressions for 1320−1600 K are

$$k_{\infty,3}(T) = 2.72 \times 10^{15} \exp(-38050\ K/T)\ [s^{-1}]$$

$$k_{0,3}(T) = 4.72 \times 10^{18} \exp(-24950\ K/T)\ [cm^3 mol^{-1} s^{-1}]$$

$$F_{cent,3}(T) = 0.28 \exp(-T/1500\ K)$$

The pressure-broadening factor, F, is given in the Troe formulation by $\log(F) = \log(F_{cent})/[1 + [(\log P_r + C)/(N - 0.14(\log(P_r) + C))]^2]$, where $N = 0.75 - 1.27\log(F_{cent})$, $C = -0.4 - 0.67\log(F_{cent})$, and $P_r = k_0[M]/k_\infty$. Figures 6−8 show the current data, RRKM calculations, and selected previous experimental studies on falloff plots; Figures 9−11 show the current high-pressure-limit rate coefficients with comparison to previous theoretical studies.

Discussion

The current experimental findings for reactions 1 and 2 can be compared with the experimental results of previous studies, Figures 6 and 7; there are no previous high-temperature experimental results for comparison to our k_3 results, Figure 8.

TABLE 2: Data Used for RRKM Calculations

	***i*-C_4H_{10}**
heat of formation (0 K)[20]	−25.43 kcal/mol
moments of inertia (amu Å^2)[21]	114.06 (inactive); 66.97 (inactive); 64.89 (active), $\sigma = 1$
frequencies (cm^{-1})[22] [a]	2987, 2921, 2898, 1469, 1388, 1171, 769, 418, 2986, 1439, 922, 204, 2990, 2978, 2914, 1465, 1445, 1361, 1314, 1152, 938, 891, 347, 248, 2990, 2978, 2914, 1465, 1445, 1361, 1314, 1152, 938, 891, 347, 428
	CH_3 ⋯ *i*-C_3H_7
frequencies (cm^{-1})[22,23] [a]	3057, 2985, 2926, 2846, 1448, 1437, 1372, 1139, 998, 854, 394, 347, 122, 2986, 2924, 2841, 1436, 1427, 1369, 1324, 1110, 910, 906, 112, 3184, 3184, 3002, 1384, 1384, 580
active 1-D external rotor (amu Å^2)[21]	64.89, $\sigma = 1$
active 1-D internal torsion (amu Å^2)[22,25] [b]	3.38, $\sigma = 3$
active 2-D internal rotor (amu Å^2)[25]	1.76, $\sigma = 2$; $\eta = 265.4-616.9\ T^{-1/6}$
active 1-D internal rotor (amu Å^2)[22] [b]	13.49, $\sigma = 1$; $\eta = 265.4-616.9\ T^{-1/6}$
active 1-D internal rotor (amu Å^2)[22] [b]	61.08, $\sigma = 1$; $\eta = 265.4-616.9\ T^{-1/6}$
barrier at 0 K[21]	86.8 kcal/mol
	***n*-C_4H_{10}**
heat of formation (0 K)[20]	−23.55 kcal/mol
moments of inertia (amu Å^2)[22] [b]	149.18 (inactive); 140.18 (inactive); 21.56 (active), $\sigma = 1$
frequencies (cm^{-1})[23]	2965, 2872, 2853, 1460, 1442, 1382, 1361, 1151, 1059, 837, 425, 2968, 2930, 1461, 1257, 948, 731, 194, 102, 2965, 2912, 1460, 1300, 1180, 803, 225, 2968, 2870, 2853, 1461, 1461, 1379, 1290, 1009, 964, 271
	CH_3 ⋯ *n*-C_3H_7
frequencies (cm^{-1})[22,23] [a]	3033, 2994, 2924, 2908, 1463, 1442, 1425, 1359, 1283, 1058, 991, 864, 506, 323, 3131, 3002, 2945, 1453, 1264, 1156, 862, 720, 246, 67, 3184, 3184, 3002, 1384, 1384, 580
active 1-D external rotor (amu Å^2)[22] [b]	21.56, $\sigma = 1$
active 1-D internal torsion (amu Å^2)[22,25] [b]	3.37, $\sigma = 3$
active 2-D internal rotor (amu Å^2)[25]	1.76, $\sigma = 2$; $\eta = 439.5-1186.5\ T^{-1/6}$
active 1-D internal rotor (amu Å^2)[22] [b]	15.40, $\sigma = 1$; $\eta = 439.5-1186.5\ T^{-1/6}$
active 1-D internal rotor (amu Å^2)[22] [b]	56.76, $\sigma = 1$; $\eta = 439.5-1186.5\ T^{-1/6}$
barrier at 0 K[20,27,28]	88.5 kcal/mol
	C_2H_5 ⋯ C_2H_5
frequencies (cm^{-1})[24]	3112, 3033, 2987, 2987, 2984, 1440, 1440, 1440, 1366, 1175, 1175, 1138, 528, 528, 528, 3112, 3033, 2987, 2987, 2984, 1440, 1440, 1440, 1366, 1175, 1175, 1138, 528, 528, 528
active 1-D external rotor (amu Å^2)[22] [b]	21.56, $\sigma = 1$
active 1-D internal torsion (amu Å^2)[22,26] [b]	12.05, $\sigma = 2$
active 1-D internal rotor (amu Å^2)[26]	4.87, $\sigma = 1$; $\eta = 282.6-672.8\ T^{-1/6}$
active 1-D internal rotor (amu Å^2)[26]	22.3, $\sigma = 1$; $\eta = 282.6-672.8\ T^{-1/6}$
active 1-D internal rotor (amu Å^2)[26]	4.87, $\sigma = 1$; $\eta = 282.6-672.8\ T^{-1/6}$
active 1-D internal rotor (amu Å^2)[26]	22.3, $\sigma = 1$; $\eta = 282.6-672.8\ T^{-1/6}$
barrier at 0 K[20,21]	87.3 kcal/mol

[a] Frequencies for *i*-C_4H_{10}, *i*-C_3H_7, and *n*-C_3H_7 are from ab initio calculations at the DFT B3LYP/6-31G** level scaled by 0.962. [b] Moments for *n*-C_4H_{10}, *i*-C_3H_7, and *n*-C_3H_7 are from ab initio calculations at the DFT B3LYP/6-31G** level.

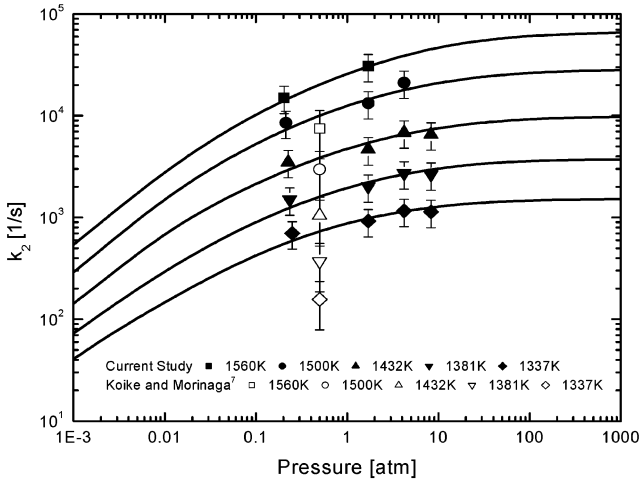

Figure 7. Falloff plot for *n*-$C_4H_{10} \rightarrow CH_3 + n$-$C_3H_7$. Solid symbols, current study; open symbols, Koike and Morinaga;[7] solid lines, RRKM/master equation results with $\langle\Delta E\rangle_{down} = 1.2 \times (T\ [\mathrm{K}])\ \mathrm{cm}^{-1}$.

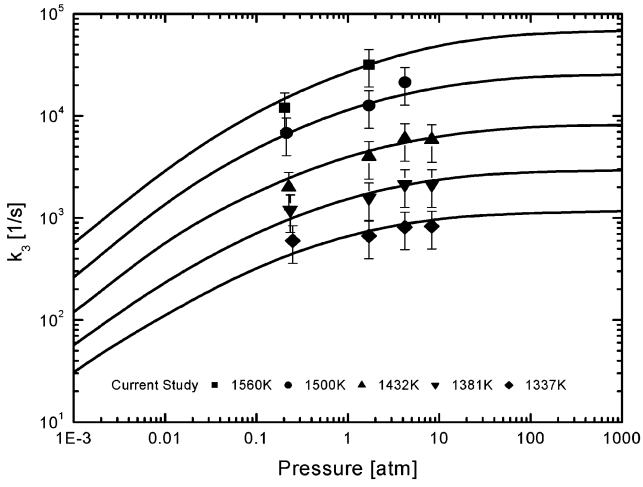

Figure 8. Falloff plot for *n*-$C_4H_{10} \rightarrow C_2H_5 + C_2H_5$. Solid symbols, current study; solid lines, RRKM/master equation results with $\langle\Delta E\rangle_{down} = 1.2 \times (T\ [\mathrm{K}])\ \mathrm{cm}^{-1}$.

The current findings for reaction 1 are in fairly good agreement with the isobutane 3.39 μm laser absorption measurements of Hidaka et al.,[5] particularly at lower temperatures. A comparison of our k_1 and k_2 results with both studies by Koike and Morinaga[6,7] shows poor agreement. Koike and Morinaga measured CH_3 using lamp absorption at 216 nm during the

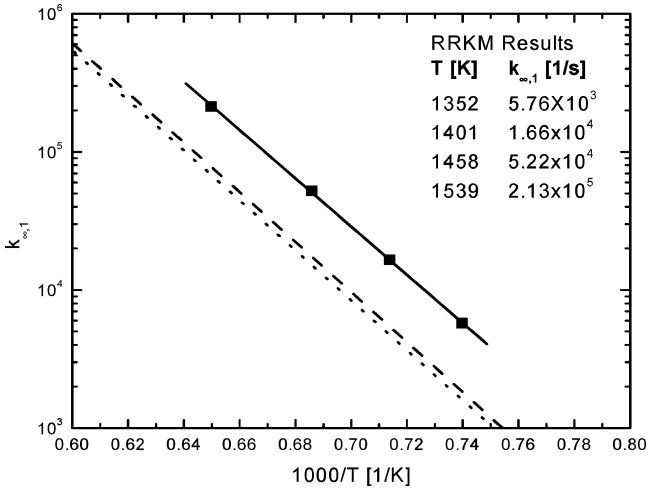

Figure 9. High-pressure rate coefficient for *i*-$C_4H_{10} \rightarrow CH_3 + i$-$C_3H_7$. Symbols, current RRKM results (listed on figure); solid line, fit to current RRKM results; dashed line, Tsang[3]; dotted line, Warnatz.[34]

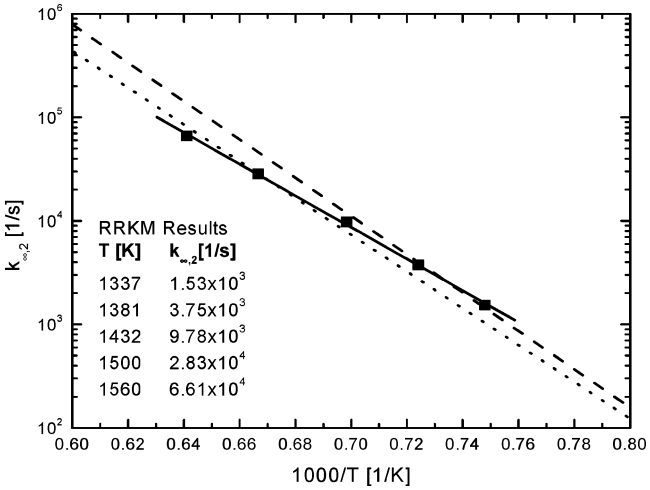

Figure 10. High-pressure rate coefficient for *n*-$C_4H_{10} \rightarrow CH_3 + n$-$C_3H_7$. Filled squares, current RRKM results (listed on figure); solid line, fit to current RRKM results; dashed line, $k_{\infty,2}$ Dean;[35] dotted line, Warnatz.[34]

shock heating of mixtures of 1−2.8% isobutane or *n*-butane diluted in argon. The large initial concentrations of reactant used in their experiments provide results that are highly sensitive to the choice of the other rate coefficients in their reaction mechanism. Their low findings for k_1 and k_2, in comparison to the current findings, is likely due to their choice of a slow rate for methyl recombination, which is of significant sensitivity in their experiments. Koike and Morinaga[6,7] employ a rate for methyl recombination that is a factor of 2 slower at 1450 K than the currently accepted rate, which has an uncertainty of ±20%.

A comparison of the current high-pressure-limit rate coefficients can be found in Figures 9−11. Our findings for $k_{\infty,1}$ are about a factor of 2 to 3 greater than the theoretical RRKM prediction of Tsang[3] and the review recommendation of Warnatz[34] but show essentially the same activation energy. The RRKM expression given by Tsang[3] was guided by the only high-temperature data available at the time, that of Koike and Morinaga,[6] thus Tsang's high-pressure-limit recommendation is lower than our finding.

The current findings for $k_{\infty,2}$ are in good agreement with the QRRK predictions of Dean[35] and the review recommendations of Warnatz[34] although our activation energy is somewhat

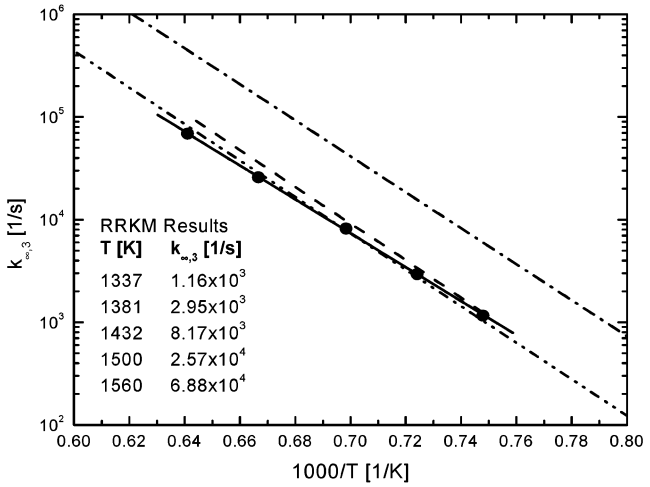

Figure 11. High-pressure rate coefficient for *n*-$C_4H_{10} \rightarrow C_2H_5 + C_2H_5$. Filled circles, current RRKM results (listed on figure); solid line, fit to current RRKM results; dashed-dot line, Dean;[35] dashed-dot-dot line, Warnatz;[34] dashed line, result using the geometric mean rule.

smaller. Recent studies on ethane decomposition[29] suggest that the rate coefficients for C−C bond fission reactions in alkanes falloff considerably more at high temperatures than previously thought. This is probably also the case for *n*-butane and could explain the difference in the activation energies of the current findings and those of Dean. The current findings for $k_{\infty,3}$ are about a factor of 3 smaller than the QRRK predictions of Dean[35] but in good agreement with the review recommendations of Warnatz.[34] The results of the current study for reactions 2 and 3 give a branching ratio, $k_2/(k_2 + k_3)$, that is approximately 0.5 (1320−1600 K), in agreement with the recommendation of Warnatz.[34]

Additionally, the current measurement of k_3 and previous determinations[3] of the rate coefficients for $C_2H_6 \rightarrow CH_3 + CH_3$ and $C_3H_8 \rightarrow CH_3 + C_2H_5$, allow a test of the validity of the geometric mean rule.[30,36,37] The geometric mean rule is often used to predict rate coefficients for decomposition or radical cross reactions, when data is not available and is written

$$k_{AB} = 2(k_{AA}k_{BB})^{1/2}$$

where k_{AB} is the rate coefficient of A + B, k_{AA} is the rate coefficient of A + A, and k_{BB} is the rate coefficient of B + B. This equation can easily be arranged for the k_3 rate coefficient, determined in this study, in terms of the previously measured rate coefficients for $C_2H_6 \rightarrow CH_3 + CH_3$ and $C_3H_8 \rightarrow CH_3 + C_2H_5$ and the appropriate equilibrium constants. The resulting rate coefficient for reaction 3 predicted by the geometric mean rule is in reasonable agreement with the current measurements, see Figure 11. This test, although limited, suggests that the geometric mean rule is a good estimator for high-temperature alkane decomposition rates.

Conclusions

Laser absorption of methyl radicals at 216.6 nm offers a sensitive method to determine the decomposition rates for isobutane and *n*-butane. Determinations of k_1-k_3 have been made in the falloff regime with experimental conditions ranging from 1297 to 1601 K and 0.20 to 8.8 atm. This is the first study in which these reactions have been studied using adequately dilute mixtures in order to sufficiently isolate the decomposition reactions. Additionally, this study provides the first high-temperature determination of k_3. Calculations based on RRKM

theory and the 1-D (internal energy) master equation were performed and fit to the current data set. Expressions are given for the high- and low-pressure-limit rate coefficients as well as Troe-formulated falloff parameters.

Acknowledgment. The present work was supported by the U.S. Department of Energy under the University Consortium on Homogeneous Charge Compression Ignition Engine Research. The authors thank David M. Golden of Stanford University for helpful discussions.

References and Notes

(1) Davidson, D. F.; Herbon, J. T.; Horning, D. C.; Hanson, R. K. *Int. J. Chem. Kinet.* **2001**, *33*, 775.

(2) Oehlschlaeger, M. A.; Davidson, D. F.; Herbon, J. T.; Hanson, R. K. *Int. J. Chem. Kinet.* **2003**, *36*, 67.

(3) Tsang, W. *Combust. Flame* **1989**, *78*, 71.

(4) Bradley J. N. *Proc. R. Soc. London, Ser. A* **1974**, *337*, 199.

(5) Hidaka Y.; Fujiwara, M.; Oki, T.; Kawano, H. *Chem. Phys. Lett.* **1988**, *144*, 570.

(6) Koike, T.; Morinaga, K. *Bull. Chem. Soc. Jpn.* **1982**, *55*, 690.

(7) Koike, T.; Morinaga, K. *Bull. Chem. Soc. Jpn.* **1981**, *54*, 2439.

(8) Golden, D. M.; Alfassi, Z. B.; Beadle, P. C. *Int. J. Chem. Kinet.* **1974**, *6*, 359.

(9) Hughes, D. G.; Marshall, R. M.; Purnell, J. H. *J. Chem. Soc., Faraday Trans. 1* **1974**, *70*, 594.

(10) Pratt, G.; Rogers, D. *J. Chem. Soc., Faraday Trans. 1* **1979**, *75*, 2688.

(11) Stewart, P. H.; Larson, C. W.; Golden, D. M. *Combust. Flame* **1989**, *75*, 25.

(12) Stewart, P. H.; Smith, G. P.; Golden, D. M. *Int. J. Chem. Kinet.* **1989**, *21*, 923.

(13) Davidson, D. F.; Chang, A. Y.; DiRosa, M. D.; Hanson, R. K. *J. Quant. Spectrosc. Radiat. Transfer* **1993**, *49*, 559.

(14) Davidson, D. F.; DiRosa, M. D.; Chang, E. J.; Hanson, R. K. *J. Quant. Spectrosc. Radiat. Transfer* **1995**, *53*, 581.

(15) Wang, S.; Miller, D. L.; Cernansky, N. P.; Curran, H. J.; Pitz, W. J.; Westbrook, C. K. *Combust. Flame* **1999**, *118*, 415.

(16) Marinov, N. M.; Pitz, W. J.; Westbrook, C. K.; Vincitore, A. M.; Castaldi, M. J.; Senkan, S. M.; Melius, C. F. *Combust. Flame* **1998**, *114*, 192.

(17) Kee, R. J.; Rupley, F. M.; Miller, J. A. *Chemkin-II: A Fortran Chemical Kinetics Package for the Analysis of Gas-Phase Chemical Kinetics*; Report No. SAND89-8009; Sandia National Laboratories: Livermore, CA, 1989.

(18) Lutz, A. E.; Kee, R. J.; Miller, J. A. *Senkin: A Fortran Program for Predicting Homogeneous Gas-Phase Chemical Kinetics with Sensitivity Analysis*; Report No. SAND87-8248; Sandia National Laboratories: Livermore, CA, 1988.

(19) Hippler, H.; Troe, J.; Wendelken, H. J. *J. Chem. Phys.* **1983**, *78*, 6709.

(20) Frenkel, M.; Marsh, K. N.; Wilhoit, R. C.; Kabo, G. J.; Roganov, G. N. *Thermodynamics of Organic Compounds in the Gas State*; Thermodynamics Research Center: College Station, TX, 1994.

(21) Lide, D. R., Jr. *Handbook of Chemistry and Physics*, 80th ed.; CRC Press: Boca Raton, FL, 1999−2000.

(22) Johnson, R. D., III, Ed. *Computational Chemistry Comparison and Benchmark Database*, Release 9; National Institute of Standards and Technology: Washington, DC, 2003; http://srdata.nist.gov/cccbdb/.

(23) Shimanouchi, T. *Tables of Molecular Vibrational Frequencies Consolidated;* Vol. 1; NSRDS NBS-39: Washington, DC, 1972.

(24) Jacox, M. E. *J. Phys. Chem. Ref. Data*, Monograph 3, 1994; updated data in NIST Chemistry Webbook. http://webbook.nist.gov/chemistry/.

(25) Yamada, C.; Hirota, E.; Kawaguchi, K. *J. Chem. Phys.* **1981**, *75*, 5256.

(26) Mousavipour, S. H.; Homayoon, Z. *J. Phys. Chem. A* **2003**, *107*, 8566.

(27) Seetula, J. A.; Slagle, I. R. *J. Chem. Soc., Faraday Trans.* **1997**, *93*, 1709.

(28) Russell, J. J.; Seetula, J. A.; Senkan, S. M.; Gutman, D. *Int. J. Chem. Kinet.* **1988**, *20*, 759.

(29) Klippenstein, S. J.; Harding, L. B. *J. Phys. Chem. A* **1999**, *103*, 9388.

(30) Knyazev, V. D.; Slagle, I. R. *J. Phys. Chem. A* **2001**, *105*, 6490.

(31) Knyazev, V. D.; Slagle, I. R. *J. Phys. Chem. A* **2001**, *105*, 3196.

(32) Knyazev, V. D.; Tsang, W. *J. Phys. Chem. A* **2000**, *104*, 10747.

(33) Barker, J. R. *Int. J. Chem. Kinet.* **2001**, *33*, 232.

(34) Warnatz, J. *Combustion Chemistry: Rate Coefficients in the C/H/O System*; Springer-Verlang: New York, 1984.

(35) Dean, A. M. *J. Phys. Chem.* **1985**, *89*, 4600.

(36) Kerr, J. A.; Trotman-Dickenson, A. F. *Prog. React. Kinet.* **1961**, *1*, 105.

(37) Blake, A. R.; Henderson, J. F.; Kutschke, K. O. *Can. J. Chem.* **1961**, *39*, 1920.